Electronic Supplementary Material (ESI) for Journal of Materials Chemistry A. This journal is © The Royal Society of Chemistry 2022

Electronic Supplementary Information (ESI) for

Transparent, conductive and flexible MXene grid/silver nanowire hierarchical films for high-performance electromagnetic interference shielding

Meng Jin,[ab] Wei Chen,[a] Liu-Xin Liu,[b] Hao-Bin Zhang,[*a] Lvxuan Ye,[b] Peng Min[a] and Zhong-Zhen Yu[*b]

[a] *State Key Laboratory of Organic-Inorganic Composites, College of Materials Science and Engineering, Beijing University of Chemical Technology, Beijing 100029, China.*
E-mail: zhanghaobin@mail.buct.edu.cn

[b] *Beijing Key Laboratory of Advanced Functional Polymer Composites, Beijing University of Chemical Technology, Beijing, 100029, China.*
E-mail: yuzz@mail.buct.edu.cn

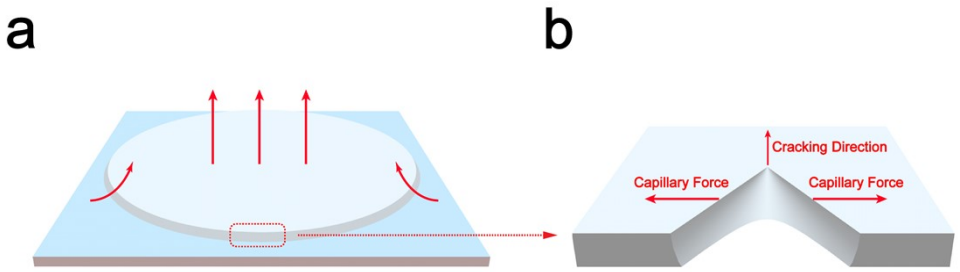

Fig. S1 Schematic illustrating (a) the evaporation process of the TiO_2 colloidal dispersion, and (b) the capillary force distribution of the dispersion at the cracking front.

With the volatilization of the dispersants, the coated TiO_2 colloidal dispersion gradually cracks to generate crack patterns under the action of capillary force. The surface evaporation of the colloidal dispersion induces a force gradient at dispersion-air interface (the capillary force less than the air pressure) during its gradual shrinkage. The dispersion is then torn apart by the capillary force to reduce the pressure, and the interactions between the dispersion and the PET substrate prevent its shrinkage. Therefore, the dispersion cracks and flows to the low-pressure zone, and the flowing distance sets the crack width.

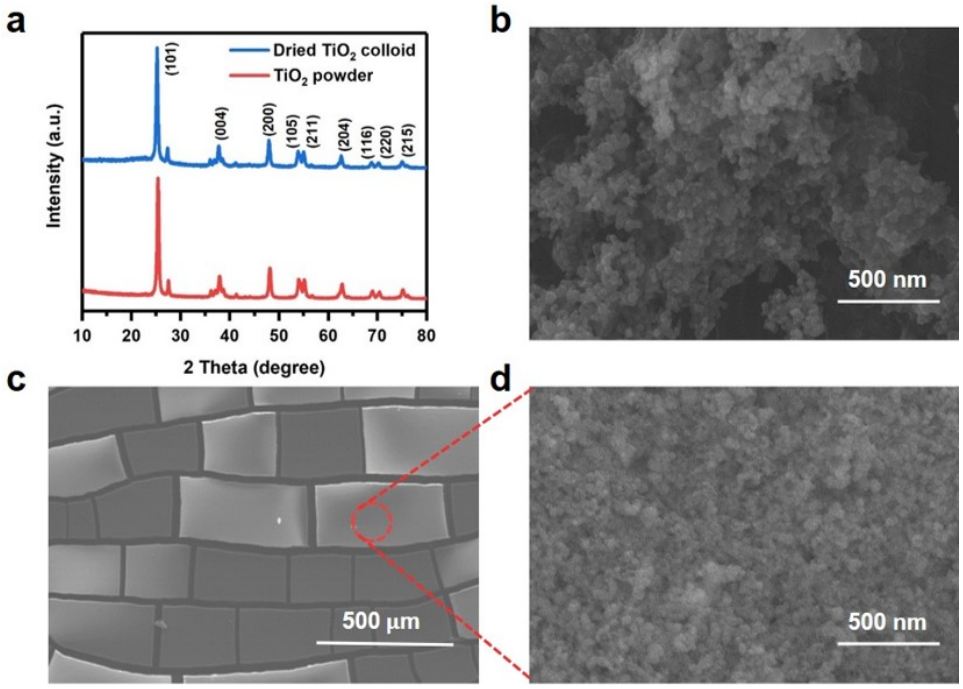

Fig. S2 (a) XRD patterns of TiO_2 powder, and dried TiO_2 colloid. SEM images of (b) TiO_2 powder, and (c, d) crack template.

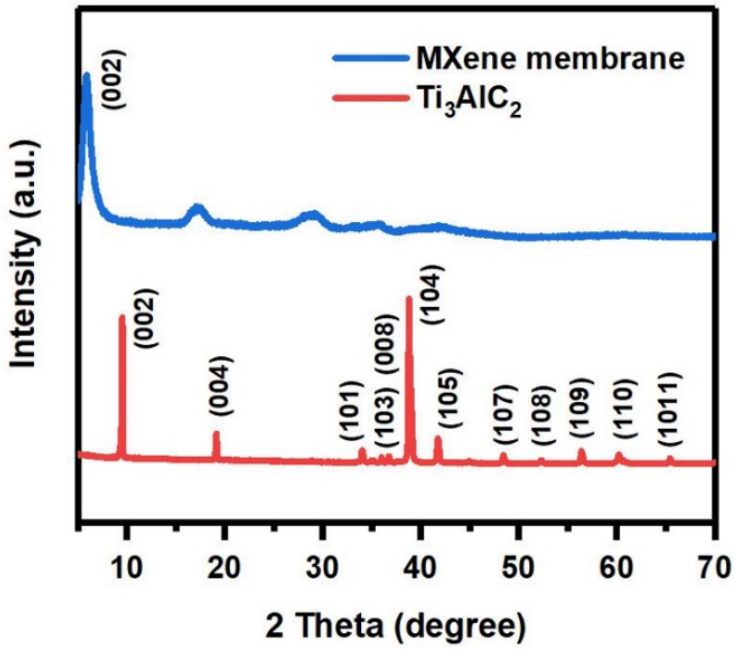

Fig. S3 XRD patterns of Ti_3AlC_2 MAX powder, and MXene membrane.

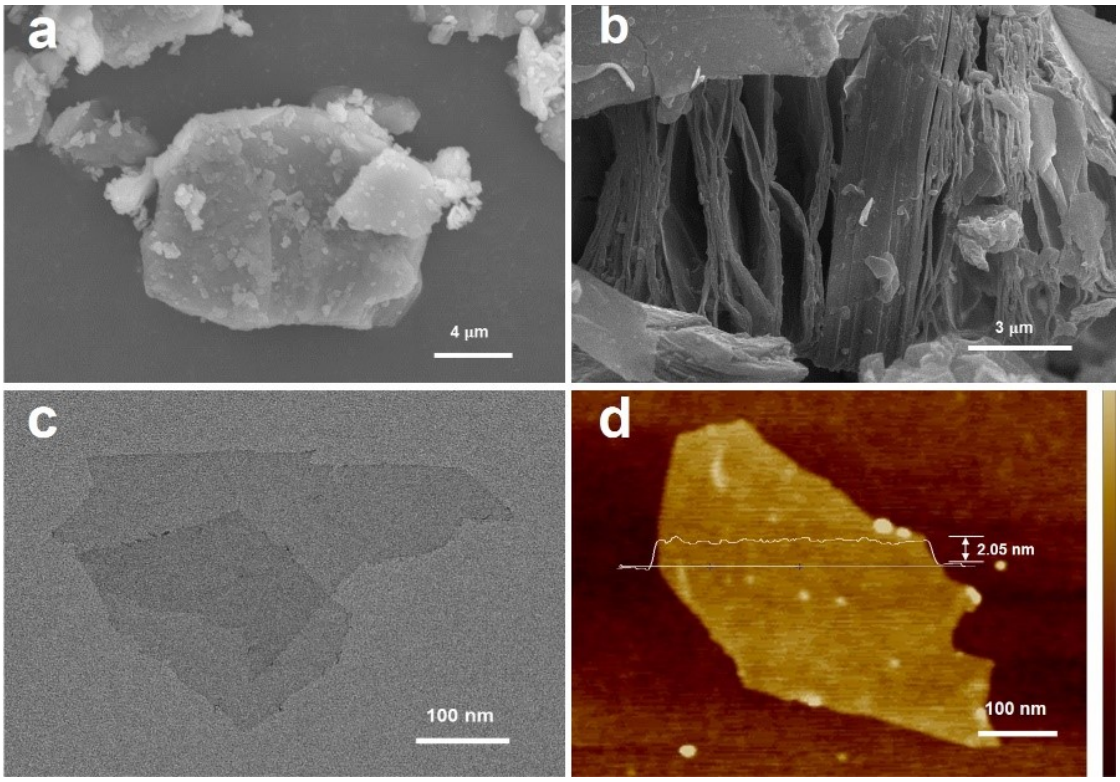

Fig. S4 SEM images of (a) Ti_3AlC_2 MAX phase, and (b) multilayered $Ti_3C_2T_x$ MXene. (c) TEM image of MXene sheets. (d) AFM image of MXene sheet.

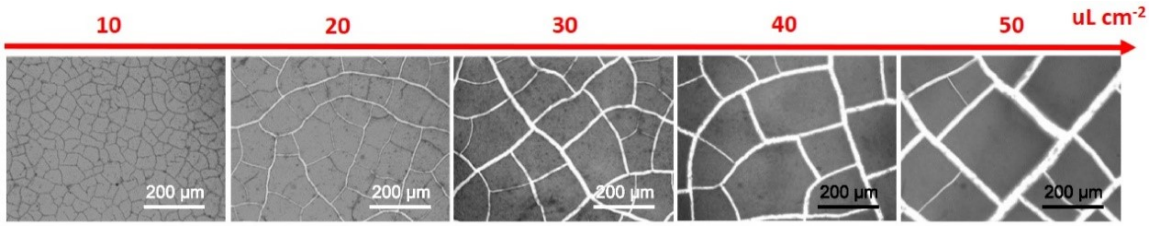

Fig. S5 Optical graphs of crack patterns at different colloidal dispersion dosages.

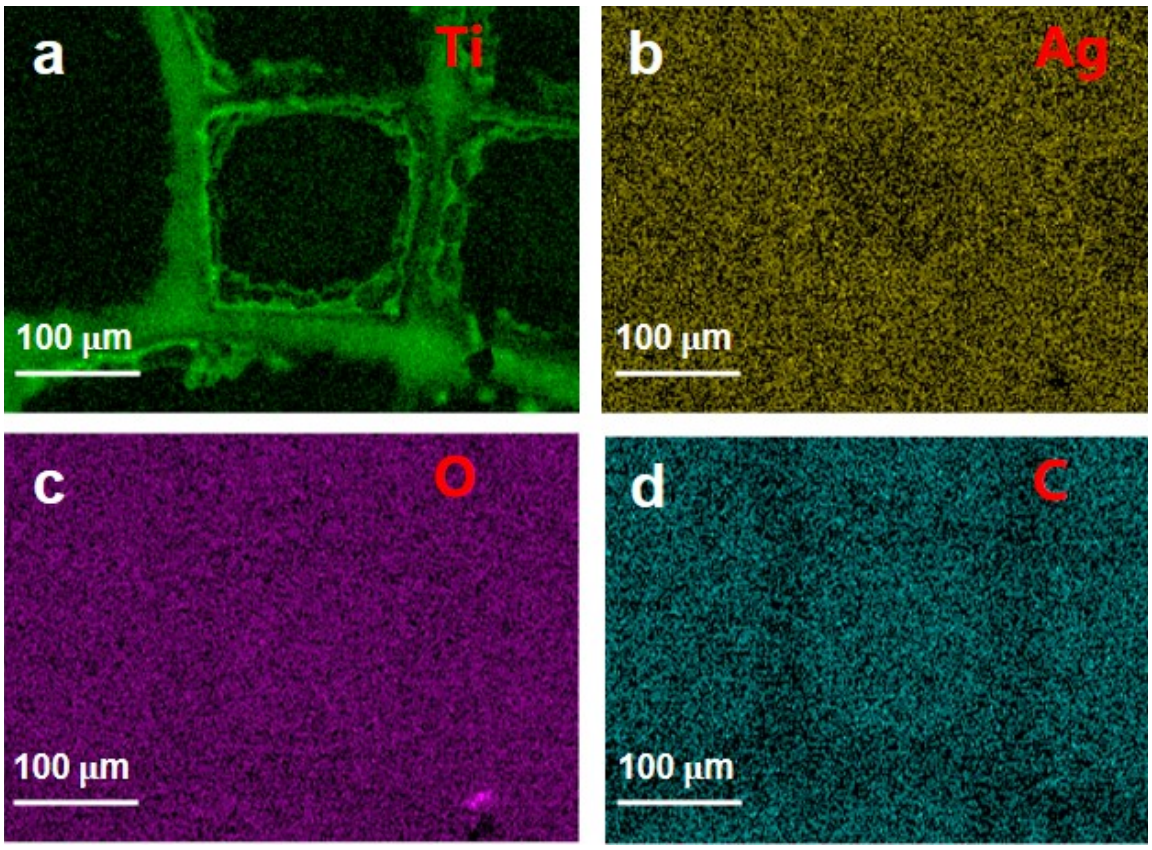

Fig. S6 EDS mapping images of (a) Ti, (b) Ag, (c) O, and (d) C elements of the MXene grid/AgNW film.

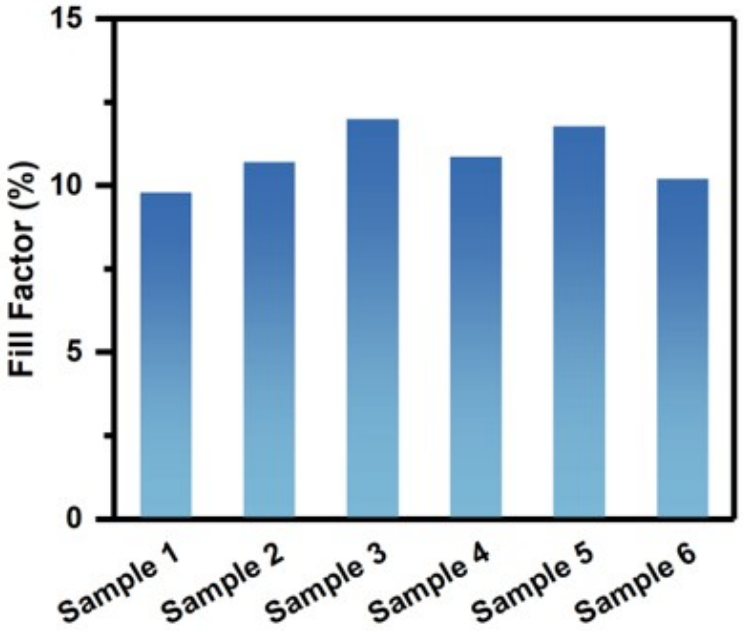

Fig. S7 Fill factors of crack templates formed at the colloidal dispersion dosage of 40 uL cm^{-2}.

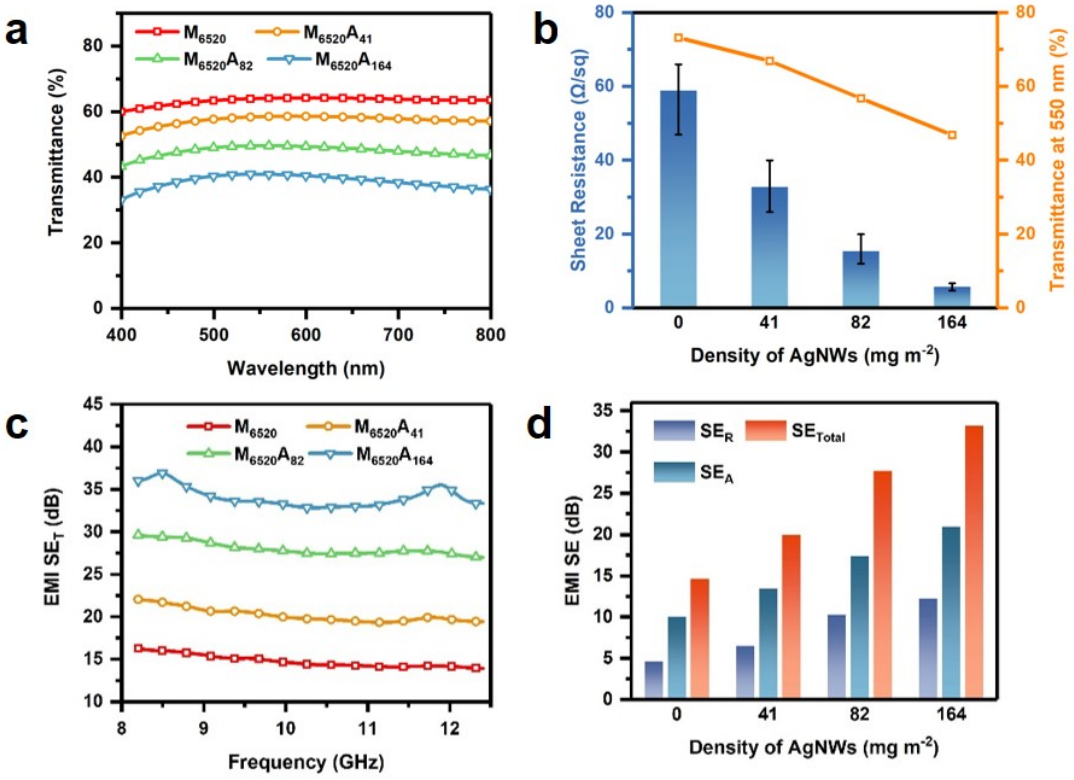

Fig. S8 (a) Optical transmittances of $M_{6520}A_n$ films in the visible light range. (b) Sheet resistances and transmittances of $M_{6520}A_n$ films. (c) Plots of EMI SE of $M_{6520}A_n$ films, and (d) the distributions of SE_R, SE_A, and SE_{Total}.

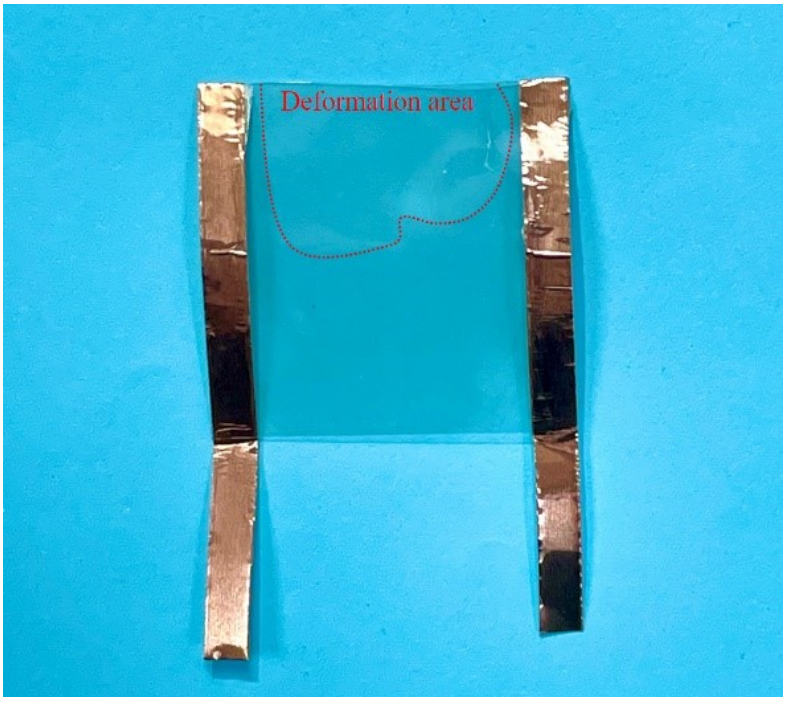

Fig. S9 The transparent heating panel is partially deformed as indicated in the circled area when the voltage is higher than 5 V.

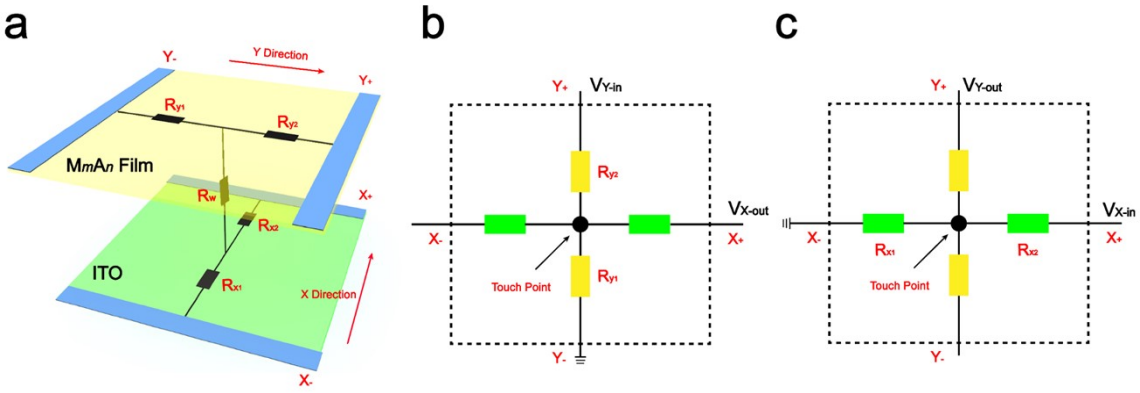

Fig. S10 Working principle of the four-wire resistive touch panel. (a) Schematic diagram of the touch panel circuit. The equivalent circuit diagrams when calculating (b) Y and (c) X coordinates.

The four-wire resistive touch panel is divided into two layers. The upper layer is a hierarchical and conductive film (M_mA_n film), while the lower layer is a conductive ITO film. On the basis of the Law of Resistance:

$$R = \rho \bullet \frac{L}{S} \tag{S1}$$

As the resistivity (ρ) and the cross-sectional area (S) of a uniform conductive film are constant,

its resistance value (R) only depends on its length (L). Fig. S10a shows the equivalent circuit of the four-wire resistive touch panel (where R_{X1}, R_{X2}, R_{Y1}, R_{Y2}, and R_W represent the resistance from the touch point to X_-, X_+, Y_-, Y_+, and the contact resistance between the upper and lower layers when touching, respectively). Since R only depends on the position of the touch point in the film, when the voltage $V_{Y\text{-}in}$ is applied in the Y-axis direction (Fig. S10b), the ordinate of the touch point can be calculated by eq. S2:

$$Y_{point} = \frac{V_{X-out}}{V_{Y-in}} \bullet H_{Y-panel} \tag{S2}$$

Where Y_{point} represents the ordinate of the touch point, $V_{X\text{-}out}$ is the voltage of the touch point measured by the chip at X_+, and $H_{Y-panel}$ stands for the height of the touch screen panel in the Y-direction. Similarly, when the voltage $V_{X\text{-}in}$ is applied in the X-axis direction, the abscissa of the touch point can be calculated with eq. S3:

$$X_{point} = \frac{V_{Y-out}}{V_{X-in}} \bullet H_{X-panel} \tag{S3}$$

Where X_{point} is the abscissa of the touch point, $V_{Y\text{-}out}$ represents the voltage of the touch point measured by the chip at Y_+, and $H_{X-panel}$ is the height of the touch screen panel in the X direction (Fig. S10c). The measured voltage is usually converted by the chip into a digital signal, which can be used as a coordinate to determine the actual position of the contact after simple processing.

Table S1. Comparison the transparent and conductive properties of MXene grid, and MXene grid/AgNW films with MXene, AgNWs, and other materials.

Materials	Matrix	Transmittance (%)	Resistance (Ω sq^{-1})	EMI SE (dB)	Refs.
$Ti_3C_2T_x$-VFM	Si	74 69 56	~3500 ~2800 ~1600	/	[1]
$Ti_3C_2T_x$-IFFT	Quartz	73	13000	/	[2]
$Ti_3C_2T_x$-DCa	Si	~56 ~41 ~29	~600 ~300 ~100	/	[3]
$Ti_3C_2T_x$-SCo	Glass	67	288	/	[4]
$Ti_3C_2T_x$-SCa	PET	12 28 44 54	6 11 25 42	/	[5]
As-deposited $Ti_3C_2T_x$	Glass	~92 ~77 ~63 ~54 ~43	1500 300 ~168 / ~100	~1.1 (10 GHz) ~4.2 (10 GHz) ~6.0 (10 GHz) ~8.1 (10 GHz) ~9.6 (10 GHz)	[6]
Heat-treated $Ti_3C_2T_x$	Glass	~92 ~77 ~63 ~54 ~43	/	~1.3 (10 GHz) ~5.6 (10 GHz) ~8.1 (10 GHz) ~10.8 (10 GHz) ~12.5 (10 GHz)	[6]
LbL MXene-MWCNT	Glass	~33	463	~2.8	[7]
LbL MXene-SWCNT	Glass	~41	503	~3.3	[7]
Reduced GO	/	60 60	~10000 ~330	/	[8]
Graphene	/	80	10492	/	[9]
AgNWs	Leaf	~86	45	/	[10]
Acrylate/AgNW	PMMA	~82	15.8	~22.5	[11]
GNS/AgNW	Glass	~78 ~67 ~43	16 9 6	~26 ~30 ~38	[12]
MXene Grid	**PET**	**86** **80**	**6004.5** **621.2**	**0.4** **2.2**	**This Work**

		74	**266.0**	**6.3**	
		68	**133.8**	**8.9**	
		64	**61.9**	**15.6**	
		61	**31.4**	**21.7**	
MXene grid/AgNW	**PET**	**83**	**50.9**	**19.1**	**This Work**
		81	**17.9**	**24.6**	
		72	**6.7**	**32.5**	

Note: $Ti_3C_2T_x$-VFM stands for MXene film obtained by vacuum filtration method; $Ti_3C_2T_x$-IFFT stands for MXene film obtained by the interfacial film formation technique; $Ti_3C_2T_x$-DCa/SCo/SCa stands for MXene film obtained by drop-casting/spin-coating/spin-casting method.

References

[1] L. Yu, A. S. R. Bati, T. S. L. Grace, M. Batmunkh and J. G. Shapter, *Adv. Energy Mater.*, 2019, **9**, 1901063.

[2] S. Chertopalov and V. N. Mochalin, *ACS Nano*, 2018, **12**, 6109-6116.

[3] Z. Kang, Y. Ma, X. Tan, M. Zhu, Z. Zheng, N. Liu, L. Li, Z. Zou, X. Jiang, T. Zhai and Y. Gao, *Adv. Electron. Mater.*, 2017, **3**, 1700165.

[4] T. H. Park, S. Yu, M. Koo, H. Kim, E. H. Kim, J. E. Park, B. Ok, B. Kim, S. H. Noh, C. Park, E. Kim, C. M. Koo and C. Park, *ACS Nano*, 2019, **13**, 6835-6844.

[5] C. J. Zhang, B. Anasori, A. Seral-Ascaso, S. H. Park, N. McEvoy, A. Shmeliov, G. S. Duesberg, J. N. Coleman, Y. Gogotsi and V. Nicolosi, *Adv. Mater.*, 2017, **29**, 1702678.

[6] T. Yun, H. Kim, A. Iqbal, Y. S. Cho, G. S. Lee, M. K. Kim, S. J. Kim, D. Kim, Y. Gogotsi, S. O. Kim and C. M. Koo, *Adv. Mater.*, 2020, **32**, 1906769.

[7] G.-M. Weng, J. Li, M. Alhabeb, C. Karpovich, H. Wang, J. Lipton, K. Maleski, J. Kong, E. Shaulsky, M. Elimelech, Y. Gogotsi and A. D. Taylor, *Adv. Funct. Mater.*, 2018, **28**, 1803360.

[8] H. A. Becerril, J. Mao, Z. Liu, R. M. Stoltenberg, Z. Bao and Y. Chen, *ACS Nano*, 2008, **2**, 463–470.

[9] X. Li, G. Zhang, X. Bai, X. Sun, X. Wang, E. Wang and H. Dai, *Nat. Nanotechnol.*, 2008, **3**, 538-542.

[10] V. Sharma, A. Koivikko, K. Yiannacou, K. Lahtonen and V. Sariola, *npj Flex. Electron.*,

2020, **4**, 27.

[11] X. Zhang, Y. Zhong and Y. Yan, *Phys. Status Solidi A*, 2018, **215**, 1800014.

[12] N. Zhang, Z. Wang, R. Song, Q. Wang, H. Chen, B. Zhang, H. Lv, Z. Wu and D. He, *Sci. Bull.*, 2019, **64**, 540-546.